Optics Letters

Continuous-wave operation of a tandem optical parametric oscillator up to 5.19 μm based on periodically poled $LiNbO_3$

Liemao Hu,[1,†] Jian Ning,[1,2,4,†] Yifan Chen,[1] Xinjie Lv,[1,*] Gang Zhao,[1] Ping Xu,[3] and Shining Zhu[1]

[1]National Laboratory of Solid State Microstructures, School of Physics, College of Engineering and Applied Science, Collaborative Innovation Center of Advanced Microstructures, Nanjing University, Nanjing 210093, China
[2]Starshining (Nanjing) Technology Company Limited, Nanjing 210043, China
[3]Institute for Quantum Information and State Key Laboratory of High Performance Computing, College of Computer Science and Technology, National University of Defense Technology, Changsha 410073, China
[4]ningjian@starshining.com
[†]The authors contributed equally to this work.
[*]lvxinjie@nju.edu.cn

Received 6 November 2023; revised 28 December 2023; accepted 10 January 2024; posted 16 January 2024; published 9 February 2024

A continuous-wave, tandem optical parametric oscillator (TOPO) based on a MgO-doped periodically poled $LiNbO_3$ (MgO:PPLN) is demonstrated. Because the MgO:PPLN is tandemly pumped by the OPO's signal beam, it outputs simultaneously two groups of signal and idler with a single pump source. The entire range spans from 1398 to 1490 nm, 1914 to 2107 nm, 3720 to 4444 nm, and 4849 to 5190 nm, which is limited by periods of the MgO:PPLN and cavity mirror coatings. The TOPO, whose oscillation threshold of pump power exceeds 7 W, can be easily triggered by marginally increasing the pump power as long as the OPO process occurs. The maximum idler powers are respectively 2.6 W (at 3896 nm) and 34 mW (at 4863 nm), and the corresponding signal powers are both nearly 100 mW.

https://doi.org/10.1364/OL.511170

Mid-infrared (MIR) laser sources operating over 2 to 5 μm have been widely applied in various fields, such as gas monitoring [1–3], molecular and chemical research [4], astronomy and cosmology [5], mass spectrometry imaging [6], and light detection and ranging (LIDAR) system [7]. Benefiting from the capability of broad wavelength tuning at MIR bands, optical parametric oscillators (OPOs) have made their way out of the laboratory into the commercial world. MgO-doped periodically poled $LiNbO_3$ (MgO:PPLN) is a commonly used nonlinear frequency conversion crystal due to its high effective nonlinear coefficient [8] and damage threshold [9]. The transparency range of the MgO:PPLN covers from the ultraviolet (UV) to MIR laser, but its transmittance drops sharply above 4.8 μm [10–12]. Thus, the performance of MgO:PPLN-based OPO at a long wavelength range (>4.8 μm) is severely limited by material absorption [13] and Manley–Rowe relations [14].

Pumped by a laser with high pulse energy, OPOs can easily generate a MIR laser near 5 μm. By changing the wavelength of the femtosecond (fs) Ti:sapphire laser, the idler outputting from a Ti:sapphire-pumped OPO was tunable above 5 μm [11,15,16]. Especially at 6.8 μm, the idler pulse duration of 100 fs and milliwatt-level average power could be achieved [16]. The picosecond (ps) OPO provided an output power of 1.1 W at 4.5 μm and was continuously tunable from 3 to 5 μm [12]. Compared to ultrashort pulse OPOs, nanosecond (ns) OPOs typically have a narrower wavelength tuning ranging from 2.8 to 4.8 μm [17–22]. The longer wavelength requires higher pump power, which is impracticable because the pump power is restricted by the damage threshold of the MgO:PPLN. Fortunately, the ns OPO's tunability can be enhanced through a tandem parametric process, namely tandem optical parametric oscillators (TOPOs) [23,24]. Based on two MgO:PPLN crystals, ns TOPOs pumped by a pulse laser could generate a cascaded idler near 5 μm [25,26]. However, using multiple separate crystals increases optical loss and requires a complex cavity design. In addition, ns TOPOs could be realized by a single crystal, and its tuning range reached 5.04 μm [27]. Similar to ns OPOs, continuous-wave OPOs (cw OPOs) are usually tunable below 4.8 μm [28–31] because of a sharp rise [32] in the oscillation threshold at longer wavelengths. A long-wave tuning range of cw MIR laser can be obtained by TOPOs. However, a cw TOPO is difficult to realize because of the complex cavity with multiple cavity mirrors and the cw pump source with low peak power.

In this Letter, we present a cw TOPO with the capacity of broad wavelength tunability. To simplify the experimental setup, the OPO and the TOPO share the same four-mirror ring cavity. The OPO is pumped by a fiber laser, and its intra-cavity signal beam tandemly pumps the MgO:PPLN to realize the TOPO. To reduce optical loss and match the mode of the cavity, a single MgO:PPLN crystal is utilized to participate twice in the frequency conversion to produce an MIR laser around 5 μm. The cw OPO generates the idler wavelength region from 3720 to 4444 nm, and the corresponding signal wavelength ranges from 1398 to 1490 nm. The other beams are generated by the TOPO,

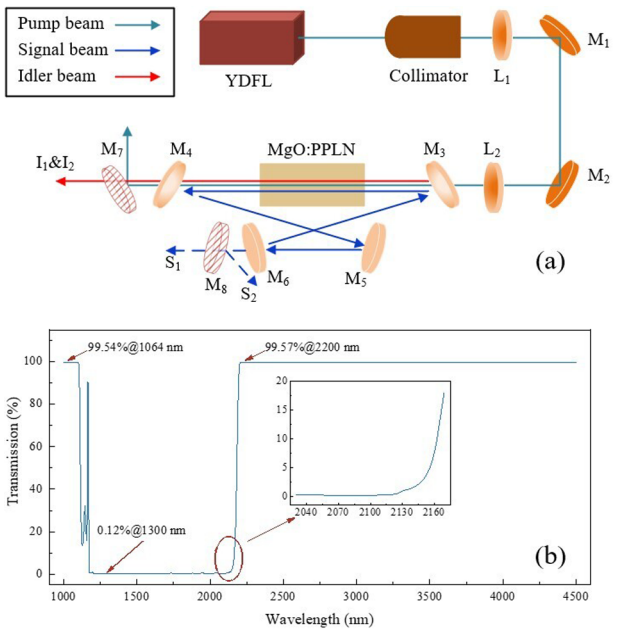

Fig. 1. (a) Experimental setup of the OPO and the TOPO. They share the same ring cavity and MgO:PPLN, but their pump sources are YDFL and the signal beam (S_1) of the OPO, respectively. YDFL, Yb-doped fiber laser; $L_{1,2}$, plano-convex lenses; $M_{1,2}$, high reflectivity mirrors, $M_{3–6}$, cavity mirrors; $M_{7,8}$, dichroic mirrors. (b) Transmission curve for cavity mirrors, and a sharp rise appears when the wavelength is beyond 2100 nm.

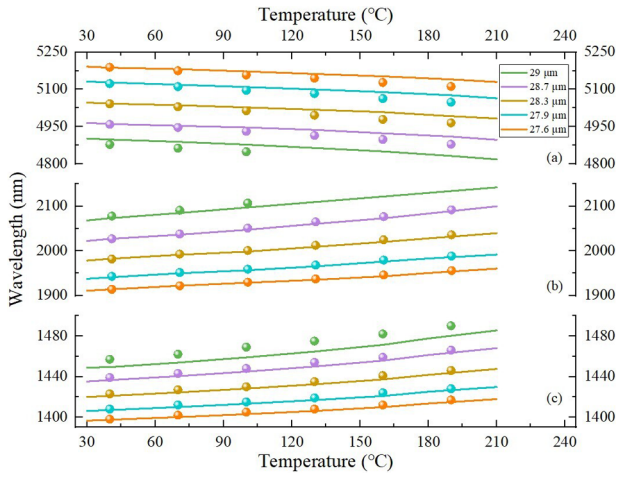

Fig. 2. Tunability of the setup. (a) TOPO's idler wavelength and (b) signal wavelength. (c) OPO's signal wavelength acts as the pump source of the TOPO. The lines and balls represent the calculated and measured results, respectively.

and their wavelength regions are from 1914 to 2107 nm and 4849 to 5190 nm. Under the pump power of 47 W, the idler of the OPO at 3896 nm has a power of 2.6 W, and its corresponding signal has a power of 118 mW (at 1462 nm). The other two beams are centered at 4863 and 2091 nm with output powers of 34 and 81 mW, correspondingly.

The experimental setup of the OPO and the TOPO is shown in Fig. 1(a). A linear-polarized cw Yb-doped fiber laser (YDFL), as the pump source of the OPO, delivers a maximum power of 50 W at 1064.02 nm with a waist size of 1.287 mm. After passing through the fiber collimator, the YDFL is reduced to a $1/e^2$ waist radius of 90 μm by two plano-convex lenses, i.e., $L_{1,2}$. It is located at the center of the nonlinear crystal to match the mode of the OPO cavity. Plate mirrors ($M_{1,2}$) are highly reflective at 1064 nm for a 45° angle of incidence. The MgO:PPLN with dimensions of $50 \times 10 \times 1$ mm^3 has ten grating periods, of which five periods are used. It has been coated accordingly for anti-reflective ($T > 99\%$) surfaces at wavelengths of 1.064 μm, 1.4 to 2.1 μm, and 2.2 to 4.4 μm. The crystal temperature is controlled by a ceramic heating plate, and its position is mounted by a linear translation stage. Similar to other cw OPOs [29,33], the four-mirror ring cavity comprises two concave mirrors ($M_{3,4}$) and two plate mirrors ($M_{5,6}$). $M_{3,4}$ with a radius of curvature of −100 mm are separated by a distance of 150 mm. The distances from M_5 to M_4 and M_6 are 105 and 55 mm, respectively. As shown in Fig. 1(b), $M_{3–6}$ are highly reflective ($R > 99.8\%$) at the range of 1.3 to 2.1 μm and transmissive ($T > 99.5\%$) near 1.0 μm and above 2.2 μm. M_7 is used to separate the idler beams from the residual pump beam and the leaking signal beams. M_8 is used to separate the two signal beams. At low pump power, the cavity is resonant at only the signal beam (S_1) of the OPO. Higher pump power can provoke oscillations of TOPO's signal beam (S_2), which results from the high intra-cavity power of S_1 pumping the MgO:PPLN tandemly. The waist sizes of S_1 and S_2 estimated by the ABCD matrix are ∼84 and ∼100 μm, respectively. The focusing parameters of S_1 and S_2 are ∼1.7, which meets the requirement that they are equal to each other and within the range of 1 to 7 [34].

In the MgO:PPLN with a single period Λ, there are two separate frequency conversion processes: $1/\lambda_p = 1/\lambda_{s1} + 1/\lambda_{i1}$ and $1/\lambda_{s1} = 1/\lambda_{s2} + 1/\lambda_{i2}$. Here, λ is the wavelength; the subscripts p, s, and i represent the pump, signal, and idler, respectively; serial numbers 1 and 2 denote the primary frequency conversion (OPO) and secondary frequency conversion (TOPO), respectively. In addition, the optical wavevectors k and Λ satisfy the equations $k_p - k_{s1} - k_{i1} = 2\pi/\Lambda$ and $k_{s1} - k_{s2} - k_{i2} = 2\pi/\Lambda$. The signal and idler wavelengths at different grating periods and temperatures can be calculated by SNLO (AS-Photonics, LLC., NM, USA) [35]. Synchronizing the course-tuning of the crystal's grating periods with the fine-tuning of the crystal's temperatures enables the setup to emit wide near- and mid-infrared radiation. Figures 2(a) and 2(b) show TOPO's idler wavelengths (4818 to 5192 nm) and signal wavelengths (1911 to 2142 nm), respectively. As shown in Fig. 2(c), the OPO's signal acts as the pump source of TOPO, of which the wavelength region is 1396 to 1485 nm. The idler of OPO with a range from 3758 to 4473 nm is omitted because the tuning curves of OPO have been reported many times.

To characterize the tunability of the setup, the output spectra of the signal and idler are measured by an optical spectrum analyzer (AQ6375C, Yokogawa Canada, Inc.) and a Fourier transform optical spectrum analyzer (OSA207, Thorlabs, Inc.), respectively. When the crystal temperature is fixed at 40°C, the signal spectra at different grating periods are shown in Fig. 3(a). Similarly, Fig. 3(b) shows the idler spectra at different crystal temperatures but with a fixed grating period of 27.6 μm. The idler spectra intensity of the OPO is higher than the TOPO's, and a longest wavelength up to 5190 nm is obtained. The symmetrical peaks near 4346 nm might result from the difference frequency generating (DFG) between the Raman shift of S_1 and the pump beam [33,36]. All data are shown as the balls in Fig. 2

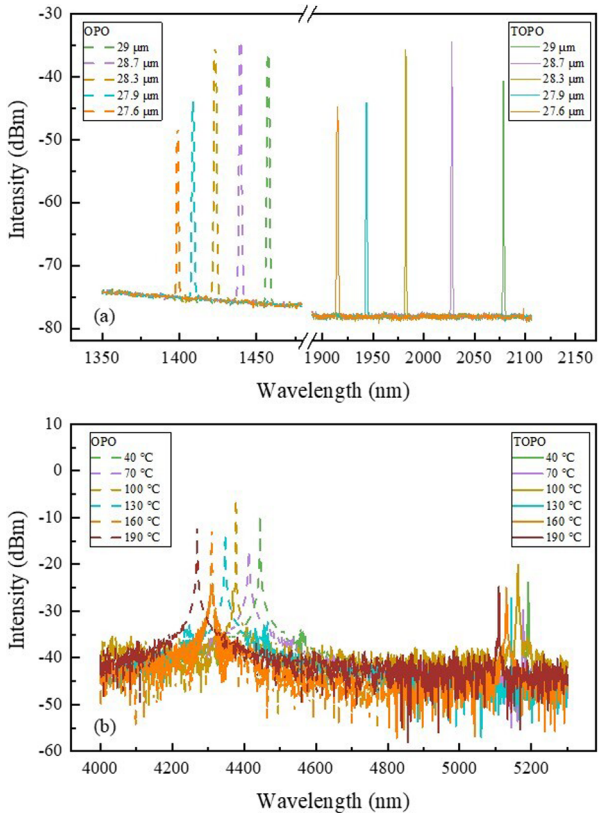

Fig. 3. Output spectra at the oscillation threshold of the pump power. (a) Signal spectra at the crystal temperature of 40°C for different grating periods. (b) Idler spectra at the grating period of 27.6 μm for different crystal temperatures.

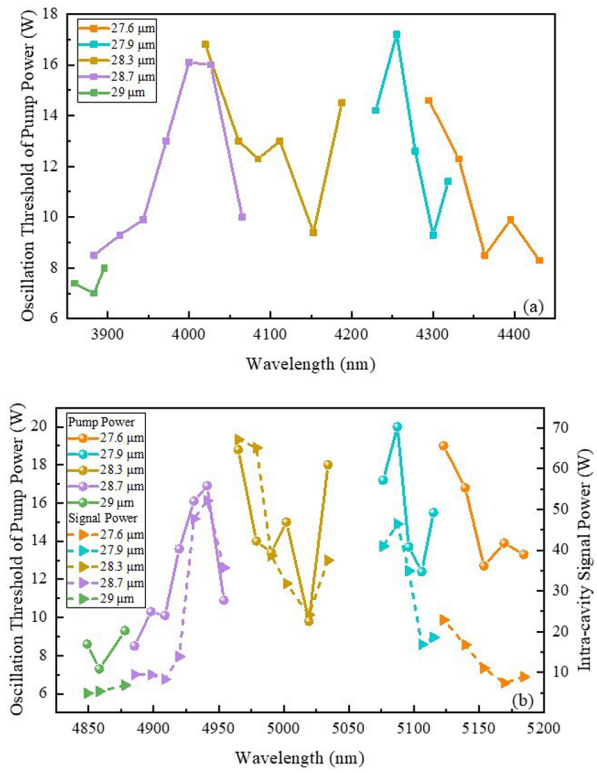

Fig. 4. (a) Oscillation threshold of pump power for the OPO in dependence on the idler wavelength. (b) Oscillation threshold of pump power for the TOPO, and intra-cavity signal power of the OPO that is estimated by measuring the signal power leaking from M_6.

to verify the estimated values. Roughly speaking, similar trends are observable between the theoretical and experimental results. However, the deviation, which has also been discovered in other published works [19,22], gradually increases with the elevation of the crystal temperature. At the grating period of 29 μm, the signal of the TOPO above 100°C is missing because the transmission above 2100 nm of cavity mirrors increases.

Figure 4(a) demonstrates the oscillation threshold of the pump power for the OPO. Typically, the power threshold below 3900 nm declines significantly when compared to other wavelengths because of the lower absorption of the MgO:PPLN below 3900 nm. Besides, a huge loss of the signal around 1445 nm due to the OH^- absorption [37] leads to a corresponding peak around 4030 nm. As the wavelength increases beyond 4225 nm, there is a slight decrease in the threshold due to a reduction in the absorption coefficient [12]. The balls in Fig. 4(b) show the threshold of the pump power for the TOPO, which will be reduced, even equal to the OPO's, if both the end faces of the crystal are antireflection-coated ($T > 99\%$) at the band region beyond 4800 nm. The TOPO can be easily triggered by marginally increasing the pump power as long as the OPO process occurs. When the S_2 of the TOPO starts to oscillate, we measure the S_1 power leaking from M_6 to estimate the intra-cavity signal power, of which the experimental data is depicted as triangles in Fig. 4(b). Because the intra-cavity signal power increases when the pump power increases, it exhibits roughly the same trend as the threshold of the pump power for the OPO. At the period of 29 μm, the oscillation threshold of the S_1 power for TOPO is ~10 W, which is in agreement with the theoretical threshold power estimated by the formula for singly resonant OPO [38].

At a fixed crystal temperature of 70°C and for a grating period of 29 μm, the output powers of the OPO and the TOPO are measured by a thermal power sensor (S425C, Thorlabs, Inc.). The power scaling results as a function of the pump power are presented in Fig. 5. For the pump power of 47 W, the OPO generates 118 mW of signal power at a wavelength of 1462 nm, together with 2.6 W of the idler power at a wavelength of 3896 nm. In addition, the wavelengths of the signal and idler generated by the TOPO are, respectively, 2091 and 4863 nm, corresponding with maximum output powers of 81 and 34 mW. The primary performance of the setup is broad wavelength tunability at the cost of low optical–optical conversion. Higher power of the TOPO might be obtained by using a crystal that is antireflection-coated at related wavelengths. The M^2 factors of the idler beams along the horizontal and vertical directions are, respectively, ~1.75 and ~1.93, which are estimated according to their diameters around the beam waist.

In conclusion, we have shown that cw TOPOs based on the MgO:PPLN can be used for obtaining MIR laser up to 5.19 μm. Although cw pump power with low peak power is difficult to realize tandem frequency conversion, the intra-cavity signal of the OPO provides gratification to the requirement of high power for the TOPO. Using the intra-cavity signal to tandemly pump the MgO:PPLN, the long-wave tuning range can be obtained with a single pump source. Moreover, the OPO and the TOPO share the same four-mirror ring cavity, which not only reduces

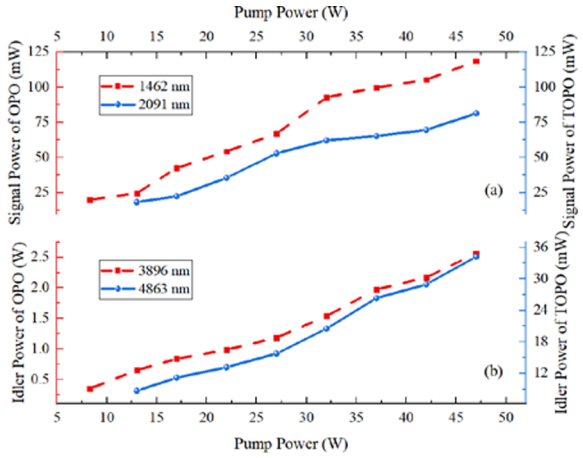

Fig. 5. Output power of the OPO (red) and TOPO (blue). (a) Signal power and (b) idler power. The grating period and the temperature of the crystal are 29 μm and 70°C, respectively. The signal beams, passing through a dichroic mirror, are measured directly by the power meter. The total power of the two idler beams is also measured by the power meter, and their power ratio is measured by the Fourier transform optical spectrum analyzer.

their oscillation thresholds but also simplifies the entire structure. Thanks to the coincidence that a single grating period meets simultaneously the quasi-phase-matching (QPM) conditions of the OPO and the TOPO, a single MgO:PPLN can participate in the frequency conversion two times. Compared with multiple crystals, a single MgO:PPLN is convenient for designing a cavity and decreasing optical loss. In addition, the whole crystal can offer efficient and robust frequency conversions for the OPO and the TOPO, which is impossible for a tandem MgO:PPLN. The setup outputs two idler beams spanning from 3720 to 4444 nm and 4849 to 5190 nm together with two corresponding signal beams, which are achieved by adjusting the temperatures and grating periods of the MgO:PPLN. We obtain 2.6 W power at 3896 nm and 34 mW power at 4863 nm. To further extend the emission range and improve the output power, we plan to redesign the crystals with other grating periods and customize the cavity mirrors in the future.

Funding. National Key Research and Development Program of China (2022YFF0712801); National Natural Science Foundation of China (12192251); National Postdoctoral Program for Innovative Talents (BX201700117).

Disclosures. The authors declare no conflicts of interest.

Data availability. Data underlying the results presented in this paper are not publicly available at this time but may be obtained from the authors upon reasonable request.

REFERENCES

1. M. W. Todd, R. A. Provencal, T. G. Owano, *et al.*, Appl. Phys. B: Lasers Opt. **75**, 367 (2002).
2. C. S. Goldenstein, R. M. Spearrin, J. B. Jeffries, *et al.*, Prog. Energy Combust. Sci. **60**, 132 (2017).
3. W. Ren, A. Farooq, D. F. Davidson, *et al.*, Appl. Phys. B **107**, 849 (2012).
4. A. L. Gomez, J. Park, M. L. Walser, *et al.*, J. Phys. Chem. A **110**, 3584 (2006).
5. F. Cataldo, D. A. Garcia-Hernandez, and A. Manchado, Mon. Not. Roy. Astron. Soc. **429**, 3025 (2013).
6. M. C. Bagley, M. Ekelof, and D. C. Muddiman, J. Am. Soc. Mass Spectrom. **31**, 319 (2020).
7. P. Weibring, H. Edner, and S. Svanberg, Appl. Opt. **42**, 3583 (2003).
8. M. H. Dunn and M. Ebrahimzadeh, Science **286**, 1513 (1999).
9. Y. Furukawa, K. Kitamura, A. Alexandrovski, *et al.*, Appl. Phys. Lett. **78**, 1970 (2001).
10. Y. R. Niu, X. Yan, J. X. Chen, *et al.*, Infrared Phys. Technol. **125**, 104243 (2022).
11. T. Andres, P. Haag, S. Zelt, *et al.*, Appl. Phys. B: Lasers Opt. **76**, 241 (2003).
12. F. Ruebel, G. Anstett, and J. A. L'Huillier, Appl. Phys. B: Lasers Opt. **102**, 751 (2011).
13. D. D. Lowenthal, IEEE J. Quantum Electron. **34**, 1356 (1998).
14. R. W. Boyd, *Nonlinear Optics*, 4th ed. (Academic Press, 2020).
15. K. C. Burr, C. L. Tang, M. A. Arbore, *et al.*, Opt. Lett. **22**, 1458 (1997).
16. P. Loza-Alvarez, C. T. A. Brown, D. T. Reid, *et al.*, Opt. Lett. **24**, 1523 (1999).
17. B. Hardy, A. Berrou, S. Guilbaud, *et al.*, Opt. Lett. **36**, 678 (2011).
18. Y. F. Peng, X. B. Wei, D. M. Li, *et al.*, Laser Phys. **22**, 87 (2012).
19. L. Xu, S. Zhang, and W. Chen, Opt. Lett. **37**, 743 (2012).
20. S. D. Liu, Z. W. Wang, B. T. Zhang, *et al.*, Chin. Phys. Lett. **31**, 024204 (2014).
21. N. Dixit, R. Mahendra, O. P. Naraniya, *et al.*, Opt. Laser Technol. **42**, 18 (2010).
22. O. Gayer, Z. Sacks, E. Galun, *et al.*, Appl. Phys. B **91**, 343 (2008).
23. X. B. Wei, Y. F. Peng, W. M. Wang, *et al.*, Chin. Opt. Lett. **8**, 1061 (2010).
24. K. J. McEwan and J. A. C. Terry, Opt. Commun. **182**, 423 (2000).
25. B. Wu, D. Z. Yang, P. P. Jiang, *et al.*, Laser Phys. **19**, 1383 (2009).
26. L. Xia, H. Su, and S. Ruan, Chin. Opt. Lett. **7**, 1038 (2009).
27. M. Vaidyanathan, R. C. Eckardt, V. Dominic, *et al.*, Opt. Express **1**, 49 (1997).
28. C. Y. Cho and Y. F. Chen, IEEE J. Sel. Top. Quantum Electron. **28**, 1500206 (2022).
29. L. M. Hu, Y. Z. He, X. J. Lv, *et al.*, Photonics **10**, 5 (2023).
30. J. W. Thomas, A. Polak, G. M. Bonner, *et al.*, Opt. Express **28**, 4550 (2020).
31. M. van Herpen, S. E. Bisson, and F. J. M. Harren, Opt. Lett. **28**, 2497 (2003).
32. L. E. Myers and W. R. Bosenberg, IEEE J. Quantum Electron. **33**, 1663 (1997).
33. M. Vainio, J. Peltola, S. Persijn, *et al.*, Opt. Express **16**, 11141 (2008).
34. G. Boyd and D. Kleinman, J. Appl. Phys. **39**, 3597 (1968).
35. A. V. Smith, "Crystal nonlinear optics with SNLO examples," AS Photonics, 2023, https://as-photonics.com/products/snlo/.
36. M. K. Shukla, P. S. Maji, and R. Das, Opt. Lett. **41**, 3033 (2016).
37. N. Waasem, S. Fieberg, J. Hauser, *et al.*, Rev. Sci. Instrum. **84**, 023109 (2013).
38. R. L. Sutherland, *Handbook of Nonlinear Optics* (CRC Press, 2003).